Journal of Petroleum Science and Engineering 207 (2021) 109091

Contents lists available at ScienceDirect

Journal of Petroleum Science and Engineering

journal homepage: www.elsevier.com/locate/petrol

Controlling factors of lamellation fractures in marine shales: A case study of the Fuling Area in Eastern Sichuan Basin, China

Xiang Xu [a,b], Lianbo Zeng [a,b,*], He Tian [a,b], Kegang Ling [c], Shiqi Che [d], Xiao Yu [e], Zhiguo Shu [d], Shaoqun Dong [a,f]

[a] State Key Laboratory of Petroleum Resources and Prospecting at China Petroleum University, Beijing, 102249, China
[b] College of Geosciences, China University of Petroleum, Beijing, 102249, China
[c] College of Engineering and Mines, University of North Dakota, Grand Forks, ND, 58202, USA
[d] Research Institute of Petroleum Exploration and Development, SINOPEC Jianghan Oilfield Company, Wuhan, Hubei, 430223, China
[e] College of Natural Sciences and Mathematics, University of Houston, Houston, TX, 77204, USA
[f] College of Science, China University of Petroleum, Beijing, 102249, China

ARTICLE INFO

Keywords:
hale
Wufeng formation-longmaxi formation
Sichuan basin
Lamellation fractures
Control factor

ABSTRACT

The lamellation fractures in marine shales are important to the accumulation and preservation of shale gas, whose characteristics and controlling factors are still unclear. This paper focus on the characteristics descriptions and controlling factor analyses based on core observations, thin sections, and scanning electron microscope (SEM) experiments. The marine shales of Paleozoic Wufeng Formation and Longmaxi Formation in the Fuling Area of Eastern Sichuan Basin are taken as an instance. The lamellation fractures are occurring along the direction of the lamellations, partially of them curved, bifurcated, and converged. The apertures of fractures typically range from 1 to 500 μm. Only a few (<1%) lamellation fractures are filled with quartz, calcite, pyrite, and bitumen. After a series of analyses, developments of lamellation fractures are controlled by total organic carbon (TOC), brittle minerals, laminae, and pyrite. (1) The organic matters control the formation and evolution of lamellation fractures by generating gas and resulting in overpressure. An increase in the TOC content of 1% can increase the lamellation fracture density by 0.26 cm^{-1}. (2) Brittle minerals, especially authigenic quartz, is also an important controlling factor to the development of lamellation fractures. When BI increases by 10%, the lamellation fracture density increases by 19%. (3) Besides, siliceous and carbonate laminae in the shale are more suitable for lamellation fractures to develop. When the laminae density is smaller than 4 cm^{-1}, it is easier to develop lamellation fractures with higher laminae density. However, too densely-distributed laminae will suppress the formation of lamellation fractures. (4) Higher pyrite content is good for the development of lamellation fractures. Lamellation fracture density will increase by 9%, with pyrite content increased by 1%. For the shale at the bottom of the Wufeng Formation - Longmaxi Formation, lamellation fractures develop extensively due to the high TOC and pyrite content, great brittleness, and moderate laminae density. The density of lamellation fractures decreases from the bottom to the top.

1. Introduction

The Fuling Shale Gas Field in the Sichuan Basin is the most successfully commercial shale gas play in China. (Gou et al., 2019; Nie et al., 2020). In 2018, the shale gas production has exceeded 2.0 × 10^{11} m^3 (Tian et al., 2020; Gou et al., 2020). It is the world's largest shale gas field outside North America (Yi et al., 2019). The main reservoir is the organic-rich marine shale in the Upper Ordovician Wufeng Formation (Fm) - Lower Silurian Longmaxi Fm. (Tuo et al., 2016; Xu et al., 2020). This area has experienced superimposed deformation of multiple phases of strong tectonic movements (Zhao et al., 2016) and developed complex and diverse natural fractures (Jiang et al., 2017; Zhang et al., 2020). Natural fractures always serve as important seepage channels and storage spaces, which control the accumulation and preservation of shale gas (Hill and Nelson, 2000; John, 2008; Kassis and Sondergeld, 2010). The characteristics of the nature fractures also affect the result of hydraulic fracturing and shale gas production (Gale and Holder, 2010; Rasouli and Sutherland, 2014; Ferrill et al., 2014; Fatahi et al., 2017).

* Corresponding author. State Key Laboratory of Petroleum Resources and Prospecting at China Petroleum University, Beijing, 102249, China.
E-mail address: lbzeng@sina.com (L. Zeng).

https://doi.org/10.1016/j.petrol.2021.109091
Received 23 August 2020; Received in revised form 5 June 2021; Accepted 9 June 2021
Available online 17 June 2021

Lamellation fracture is one of the most important and special natural fractures widely developed in marine shale in the Fuling Area (Guo and Zhang, 2014; Tian et al., 2020) (see Table 1).

Lamellation fractures are also named bedding fractures, bedding parallel fractures, or interlayer fractures. Recently, lamellation fractures in shales have attracted more and more attentions due to the high productions of shale gas. (Gale and Holder, 2010; Zeng et al., 2016; Zhang et al., 2019). In the paper, the lamellation fractures are referred to the natural fractures resulting from the fracturing of shale along or approximately parallel to the direction of lamellations. The shape, scale, and origin type of lamellation fractures vary and are involved. They can be generated from multiple geological processes. (Zeng et al., 2013; Wang et al., 2017). The minerals in shale are usually arranged within layers, where various minerals exhibit different compressive abilities when subjected to mechanical compaction. As a result, lamellation fractures form at different laminae interfaces or mineral interfaces (Zeng et al., 2016; Zhang et al., 2020; Gu et al., 2020). Besides, crystal structure change in some carbonate minerals or transformation among clay minerals due to pressure dissolution can also form lamellation fractures. (Jiu et al., 2013). Because of the uplift of formations, the effective stress in the vertical direction decreases, and the lamellation fractures then occur along the weak interfaces (Dewhurst et al., 2011; Zhang et al., 2020). During the hydrocarbon generation process, the acid fluids are generated and dissolve some minerals. This can change the sensitivity of the shale (Zeng et al., 2013), and cause anisotropy of primary wave (P-wave) (Allan et al., 2014), thus forming lamellation fractures. At the same time, the intrusion of acid fluids can further extend the lamellation fractures (Jiu et al., 2013; Zhang et al., 2019). Some scholars believe that weathering (Gu et al., 2020) or the crystallinity of the minerals (Gratier et al., 2012) can also result in lamellation fractures, while more investigators believe that the overpressure produced by the maturity of organic matter is the key factor to form lamellation fractures (Rozhko et al., 2007; Zeng et al., 2013; Jiu et al., 2013; Wang et al., 2016). When kerogen is converted to bitumen, a large amount of gas is released, which results in the formation of overpressure (Lash and Engelder, 2005; Jiu et al., 2013; Gale et al., 2014). The vertical gradient of overpressure produces seepage force, causing the maximum principal stress in the vertical direction to change from compression to tension (Cobbold et al., 2013), which leads to cracks along the lamellations and form lamellation fractures in shale. (Luo et al., 2016; Zhang et al., 2020).

Because of the complexity of the origin types, the development characteristics and controlling factors of the lamellation fractures are complicated and diverse (Wang et al., 2017; Zhang et al., 2019). However, lamellation fractures is only described as one of the natural fractures due to the limited researches in this area. (Guo and Zhang, 2014; Zhang et al., 2020). Quantitative characterizations about development characteristics of the lamellation fractures have lacked. In addition, there is still no systematic study on the controlling factors of the lamellation fractures. Therefore, this work is to fill the gaps in the study of lamellation fractures.

This study is to quantitatively study characteristics of lamellation fractures, including the shape, density, fracture aperture, fillings, etc., in the Paleozoic Wufeng Fm - Longmaxi Fm in the Fuling Area of Eastern Sichuan Basin. All analyses were based on observations of cores, thin sections, and scanning electron microscopy (SEM) experiments. Combining experimental analysis data of Total organic carbon (TOC) and X-ray diffraction (XRD), this study discussed the controlling factors of lamellation fractures. The results can provide a guidance for better understanding of the distribution characteristics and development rules of lamellation fractures in marine shales.

Table 1
The types of experiments and the numbers of samples and the purpose of each experiment.

Types of experiments	Numbers of shale samples	Purpose of experiments
Thin section identification (TSI)	82 samples from JY-A well	Observe the microscopic characteristics of fractures
Scanning electron microscopy(SEM)	14 samples from JY-A well	Observe the microscopic characteristics of fractures
X-ray diffraction (XRD)	191 samples (96 from JY-A Well and 95 from JY-B Well)	Obtain the mineral composition of the sample
Total organic carbon (TOC)	191 samples (96 from JY-A Well and 95 from JY-B Well)	Obtain the total organic carbon content of the sample
Core observation and description	221 m cores (112 m in JY-A Well and 109 m in JY-B Well)	Observe the macro characteristics of fractures

2. Geological settings

2.1. Tectonic backgrounds

The Fuling Area is located in Chongqing City, China. The study area belongs to the southeast of the barrier fold belt in eastern Sichuan (Fig. 1a). It is connected to the central Sichuan structural belt and bounded by the Huayingshan Fault in the west and bounded by Qiyueshan Fault at the margin of the basin in the east. (Hu et al., 2014; Guo and Zhang, 2014). Jiaoshiba block and Pingqiao block are the two main shale gas fields (Guo, 2019), located in the northeast and southwest of the study area (Fig. 1b). Jiaoshiba block is a box-shaped anticline. Its boundary is controlled by the northeast-to-southwest Diaoshuiyan Fault and Shimen Fault, and by northwest-to-southeast Daershan Fault and Wujiang Fault. The overall structural deformation is small and the strata tend to be flat (Hu et al., 2018; Nie et al., 2020). Pingqiao block is a narrow and long faulted anticline controlled by the northwest-to-southwest East Pingqiao Fault and West Pingqiao Fault. The core and southeast part of the anticline are tectonically stable and the strata tend to be relatively flat. The two limbs on east and west sides of the anticline are dipping steeply with strong tectonic deformation (Guo, 2019).

The Fuling Area has undergone multiple-phase tectonic evolution, characterized by early subsidence and late uplifting. The strata here ranged from Late Sinian to the Triassic period (Zhao et al., 2016). During the Late Ordovician, the Caledonian orogeny resulted in the strongest deformation. At the margin of Upper Yangtze Platform, the Central Sichuan Uplift, the Central Guizhou Uplift, and Xuefeng Uplift were quickly lifted and formed paleo-continent. At that time, the Fuling Area was in a semi-closed restricted continental shelf environment. (Zhang et al., 2020). During the deposition period of the Wufeng Fm - Longmaxi Fm, the study area was in an almost still large bay environment with low energy and hypoxia (Zhang et al., 2018a).

2.2. Stratigraphic units

This study targeted the Upper Ordovician Wufeng Fm and the First Member of the Longmaxi Fm of Lower Silurian. In the study area, the total thickness of the targeted layers is from 80 to 150 m (Fig. 2). In general, the targeted layers are characterized by obvious trichotomy. As shown in Fig. 2, layers ① and ⑤ are mainly black carbonaceous and siliceous shale, containing siliceous biological fossils like radiolarian and sponge spicule. Layers ⑥ and ⑦ are mainly gray-black and black silty shale. The siliceous components here are mainly terrestrial silts with rare biological fossils. Layers ⑧ and ⑨ are mainly gray and dark gray clay shale, while siliceous content is low. (Guo, 2019; Zhang et al., 2018b). From the bottom to the top, the targeted layers displayed lighter color, decreasing TOC content, fewer siliceous minerals, and increasing clay content (Tuo et al., 2016; Zhang et al., 2020).

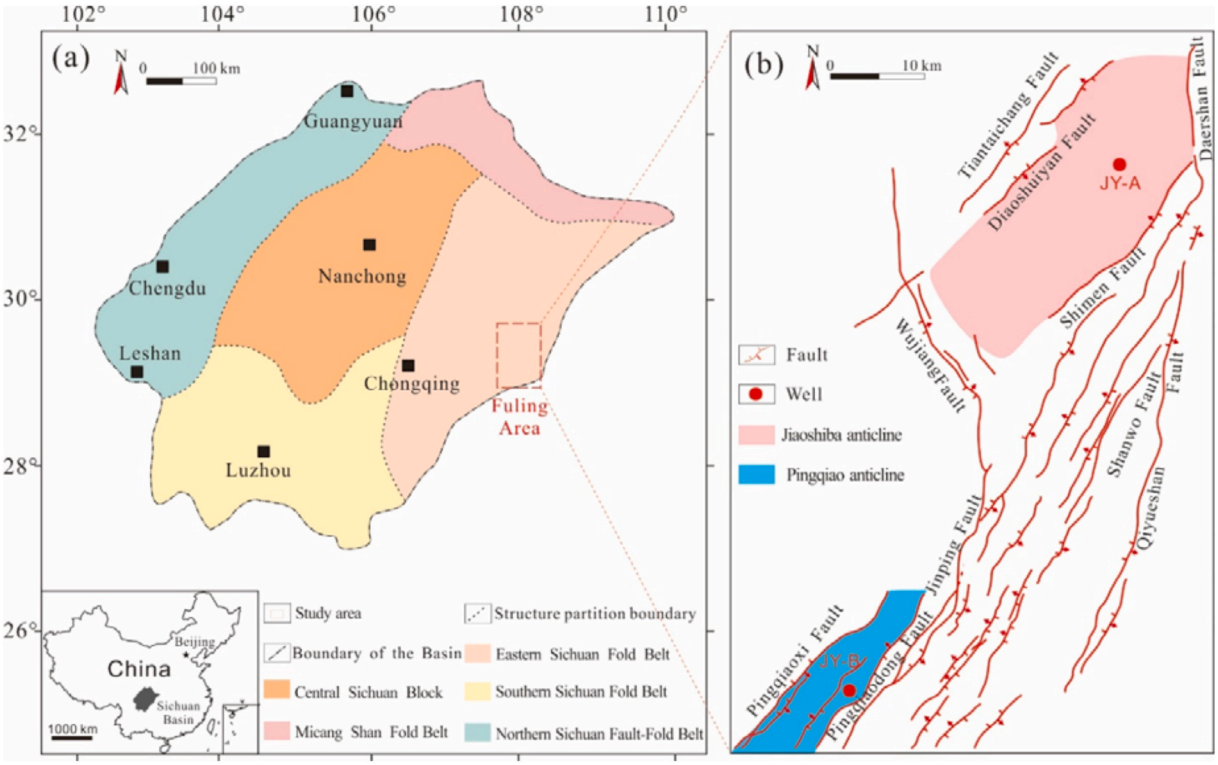

Fig. 1. (a) Location of the study area (the dotted rectangle) and tectonic units of the Sichuan Basin. (b) Structural features in the Fuling Area. The pink and blue areas show the studied anticlines and the red points are the sampling wells (modified from Nie et al., 2020). (For interpretation of the references to color in this figure legend, the reader is referred to the Web version of this article.)

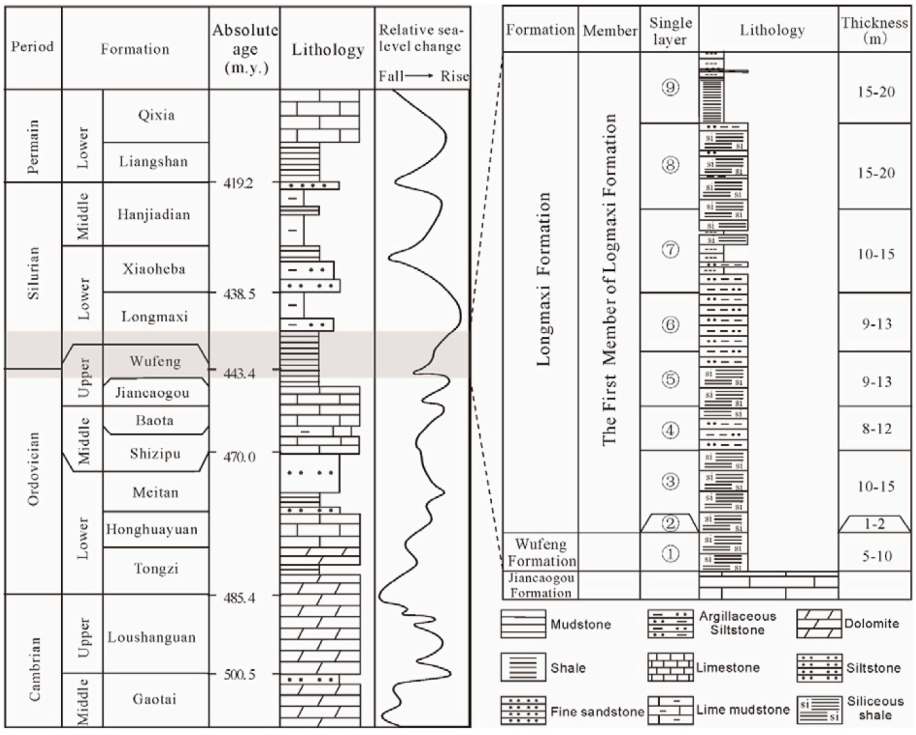

Fig. 2. The stratigraphic column in the Fuling Area including the lithological combination. The enlarged part marked by the red rectangle represents the targeted strata in this study.

3. Materials and methods

3.1. Shale samples

This paper chose two vertical wells (JY-A Well and JY-B Well) to implement core analysis. Based on the sample analyses, detailed observations and descriptions of the lamellation fractures in all cores are further conducted. The total length of the cores is 221 m (112 m in JY-A Well and 109 m in JY-B Well). The observed parts cover the entire targeted layers, including the Wufeng Fm and the Longmaxi Fm. In the JY-A Well cores, 82 samples were selected at equal intervals to do thin section identification (TSI), fourteen shale samples were selected to do scanning electron microscopy (SEM) analysis to observe the microscopic characteristics of the lamellation fractures. The sampling depth was from 2266.4 m to 2363 m. To investigate the marine shale organic petrography and mineralogy, we collected 191 shale samples (including 96 from JY-A Well and 95 from JY-B Well) of the Longmaxi Fm - Wufeng Fm in the Fuling Area. These samples were analyzed using X-ray diffraction (XRD) and total organic carbon (TOC) content test. The sampling interval is 1 m apart and samples covered the entire targeted layers.

3.2. Microscope experiment

In this study, shale samples were mechanically cut and ground into thin sections for microscopic observation. The thin sections were cut perpendicular to the plane and instilled with blue resin, and the size is 2 × 2 cm. Two thins sections were selected from each layer (from ① to ⑤) to do SEM analysis, and one thin section was chosen from layer ⑥ to ⑨. All thin sections were cut and polished perpendicular to the plane, and gold-plated lightly at the surface for electricity conduction. These experiments were all conducted in the State Key Laboratory of Petroleum Resources and Prospecting, China University of Petroleum, Beijing. All observations and analyses followed the SY/T 5162-1997 standard. TSI experiments used the Leica DM4500 polarizing microscope. SEM analysis used Quanta 200 F with a maximum resolution of 10 nm.

3.3. Organic petrography and mineralogy

TOC contents were measured using the LECO CS230 carbon and sulfur analyzer. The powder samples were prepared before testing, and approximately 200 mg of powder sample was carefully weighed for TOC measurement. Before the heating and burning analyses, all the samples were acidified using HCl to remove the inorganic carbon. Then the samples were washed using distilled water for about 24 h to clean the residual HCl and dried in a vacuum oven for about 12 h. XRD was conducted for analyses of mineral compositions quantitatively. The powder samples with grain size less than 200 mesh were performed using the BRUKER X-ray diffractometer under the temperature of 24 °C and relative humidity of 48%.

3.4. Natural fractures characterization

The description of the characteristics of natural fractures generally includes fracture type, fracture length, fracture aperture, fracture dip angle, fracture density, and fillings (Gale et al., 2007; Hooker et al., 2013; Gong et al., 2019). This study mainly focuses on density, fracture aperture, shape, and fillings. To study the density of lamellation fractures, this study mainly considered the linear density. Linear density is a measure of the quantity of lamellation fractures per unit length. (Ortega et al., 2006; Laubach et al., 2009; Zeng et al., 2010). Density mentioned in this paper is referred to linear density. This study took 1 m core depth as one unit, and counted the number of lamellation fractures and actual core length. The ratio of these two values is the density. The fracture aperture gave a precise indication of the average width of two accurately located parallel knife-edges (Marrett et al., 1999). Although when the cores were taken out of the well, fracture aperture tended to increase because of the unloading of formation pressure, it can reflect the development of lamellation fractures underground to certain extent (Zeng et al., 2010; Lyu et al., 2017; Shi et al., 2020a). Macroscopically, feeler gauge was used to measure the fracture aperture directly on the cores in the analysis. Microscopically, results of TSI and SEM experiments were further interpreted with corresponding software. Conventional core plugs were observed to characterize the shape and fillings of lamellation fractures while TSI and SEM analyses were applied to determine whether there was continuity, branches, bending, fillings, or dissolution. (Bons et al., 2012; Anders et al., 2014; Lander and Laubach, 2015; Lyu et al., 2017; Liu et al., 2020b).

4. Results

4.1. Organic petrography and mineralogy

Siliceous and clay minerals are main components in the shale samples with few carbonate minerals (Fig. 3a). The main lithology is siliceous shale. The quartz content is between 14% and 73.8%, with an average of 36.2% (Fig. 3b). The content of feldspar and carbonate minerals are relatively low, with an average of 7.8% (ranging from 2.2% to 19.4%) and 9.6% (ranging from 0 to 49.3%). The clay mineral content is between 15.6% and 68.1%, with an average of 42.8%. The average content of pyrite is 3.6% (ranging from 0.3% to 16.9%).

The brittleness index (BI) is an important indicator to quantitatively characterize the difficulty of rock fracture (Holt et al., 2015). BI can usually be calculated directly from the content of brittle minerals, but there are often multiple schemes for the selection of brittle minerals (Sone and Zoback, 2014; Gholami et al., 2016). In this study, quartz, feldspar, and carbonate minerals were used as brittle minerals to calculate the brittleness index (Wang et al., 2015; Gou et al., 2020). The specific calculation method can be found in Eq. (1).

$$BI = (W_{Qtz} + W_{Carb} + W_{Feld}) / (W_{Qtz} + W_{Carb} + W_{Feld} + W_{Clay}) \times 100\% \quad (1)$$

where BI is the brittleness index, %; W_{Qtz} is the quartz content, %; W_{Carb} is the carbonate content, %; W_{Feld} is the feldspar content, %; W_{Clay} is the clay content, %.

The shale samples in the Fuling Area show a high BI (Fig. 4a). The average BI of JY-A Well is 59.6%, with a maximum of 83.7% and a minimum of 28.9%. More than 90% samples have BI values between 40% and 80%. In the range of 60%–70%, the frequency distribution value is the highest. The BI in JY-B Well ranges from 37.7% to 78.5%, with an average of 52%, smaller than that of JY-A Well. More than 80% of the samples have a BI ranging from 40% to 60%. Vertically, the BI of all samples gradually decreases from the bottom to the top. The BI of layer ① at the bottom is 68.1%, and that of layer ⑨ at the top is 43.9%.

Shale samples have a high TOC content (Fig. 4b), with an average of 1.96%. In JY-A Well, TOC content ranges from 0.39% to 5.11%, with an average of 1.94%. There are 74% of the samples whose TOC content ranges from 2% to 4%. In JY-B Well, TOC content ranges from 0.59% to 5.55%, with an average of 2%. Samples with TOC content higher than 1% account for 98% of total samples, among which only 4% of samples with TOC content higher than 4%. The TOC content of shale samples has an obvious decreasing trend from the bottom to the top. The TOC content in layers ① and ③ at the bottom is more than 3%, while that of layers ④ and ⑤ is more than 2%, and that of top layers is below 2%.

4.2. Characteristics of lamellation fractures

Lamellation fractures are natural fractures occurring along the direction of the lamellations. (Zeng et al., 2016). They are the most common fracture types in shale reservoirs (Zhang et al., 2019). According to the core observation, these fractures are usually distributed

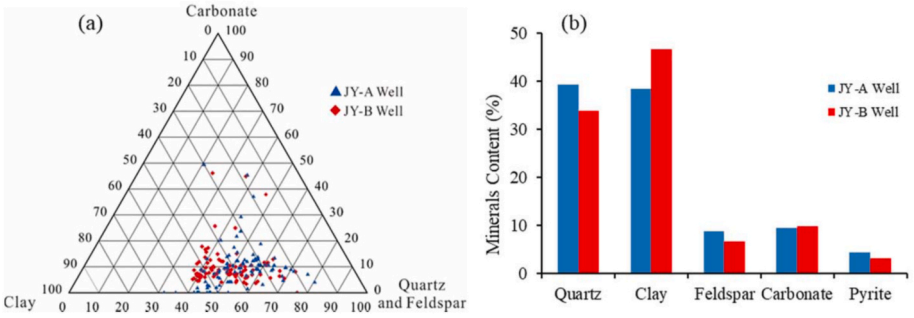

Fig. 3. (a) Triangular diagram of the mineral compositions of the shale samples from JY-A Well and JY-B Well. (b) Distribution histogram of the content of different minerals in shale samples from JY-A Well and JY-B Well.

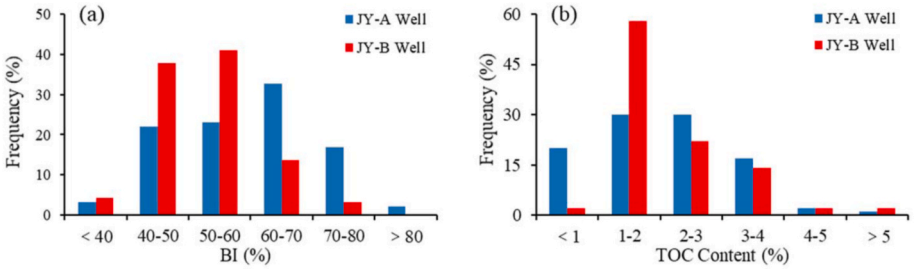

Fig. 4. (a) Frequency distribution histogram of BI of the shale samples from JY-A Well and JY-B Well. (b) Frequency distribution histogram of TOC content of the shale samples from JY-A Well and JY-B Well.

intermittently and almost parallel to the surface of the lamellations (Fig. 5a). As to their morphology, the fractures are bended and bifurcated irregularly, showing obviously equal interval distribution on the cores. The measurements of feeler gauge indicates that the fracture aperture is generally less than 0.5 mm, mainly around 0.1 mm. It can only be observed using a magnifier or wetting the cores. (Fig. 5b). The density is between 0.2 and 2 cm^{-1}. The lamellation fractures are associated with the abnormally high-pressure fractures. The fractures caused by abnormally high pressures (AF) communicate different lamellation fractures (LF) in the vertical direction to form a connecting network (Fig. 5c). Less than 1% of lamellation fractures are filled (Fig. 5c, d, 5e) by minerals including quartz, calcite, pyrite, and bitumen. The width of the filling veins is generally between 100 and 1000 μm, with the maximum reaching 1 cm. In the adjacent fractures, fillings can be different (Fig. 5d), depending on the properties of the matrix fluid when the fracture formed.

Through observations of thin sections, it is found that the lamellation fractures are usually approximately parallel to the lamellations (Fig. 6a). The fractures can be bended when close to minerals, but not cut through the minerals. They tend to extend along the edges of the particles (Fig. 6b). This is the biggest difference from shear fractures. The fracture surface of the lamellation fractures is mostly zigzag (Fig. 6a–c), obviously transformed by dissolution. This phenomenon can be observed in most lamellation fractures, indicating that the fractures are extremely susceptible to be dissolved by late acid fluids (Wang et al., 2016; Zhang et al., 2019). Lamellation fractures can be branching shown under electron microscope (Fig. 6c). A main fracture can also be bifurcating in two approximately parallel secondary branches extending forward. The

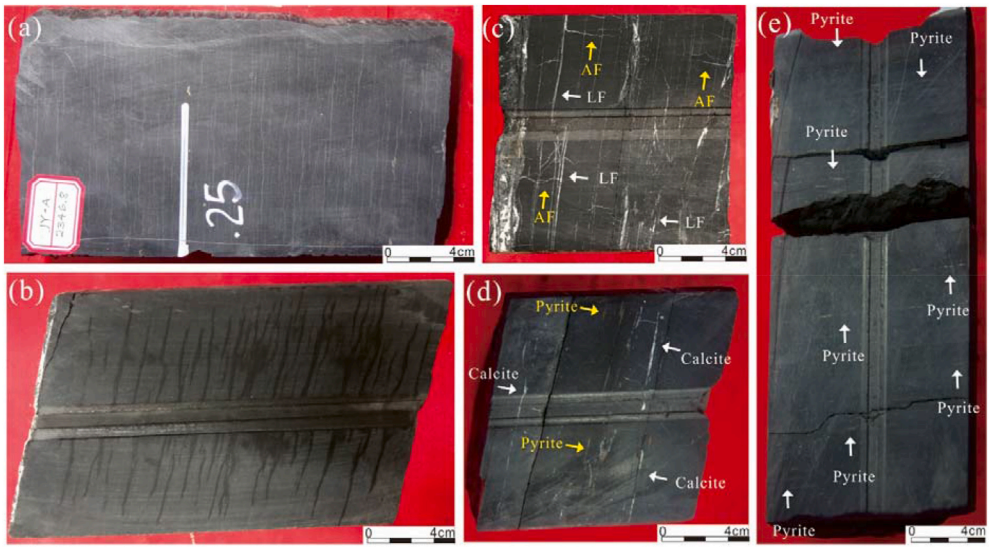

Fig. 5. Lamellation fractures in the shale cores in the Fuling Area. (a) Lamellation fractures in one shale core from JY-A Well (The depth is 2346.8 m). (b) Lamellation fractures in one wetted shale core from JY-B Well (The depth is 4033.2 m). (c) Lamellation fractures filled with quartz from JY-B Well (The depth is 4039.7 m). Some lamellation fractures (LF) connect with fractures caused by abnormally high pressures (AF) like a network. (d) Lamellation fractures filled with calcite and pyrite from JY-B Well (The depth is 4027 m). (e) Lamellation fractures filled with pyrite from JY-B Well (The depth is 4041.1 m).

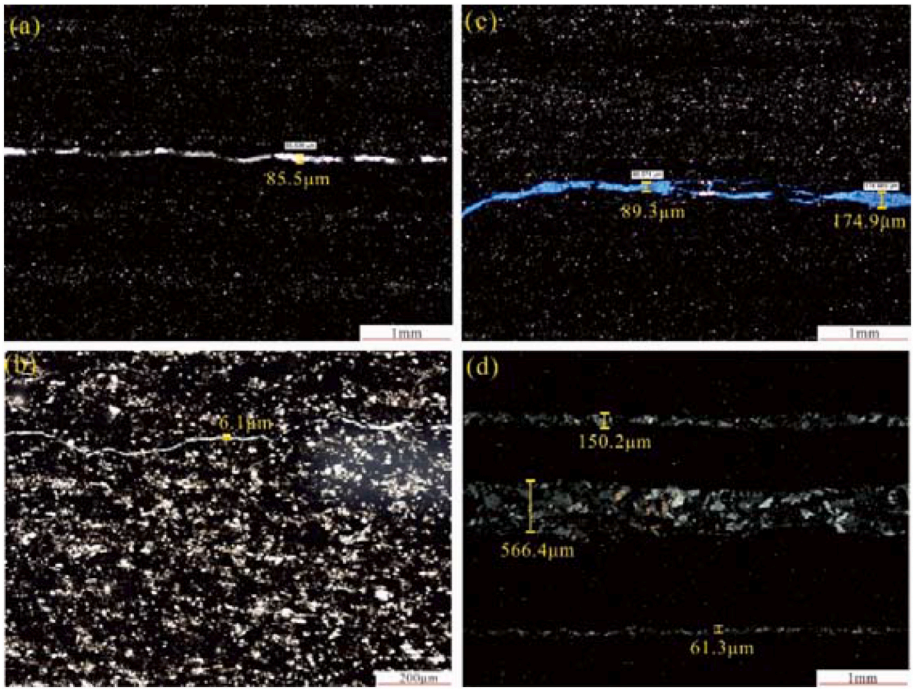

Fig. 6. Lamellation fractures observed from thin sections of the shales in the Fuling Area. (a) One lamellation fracture parallel to the lamellations in shales from JY-A Well (The depth is 2320.6 m). (b) One bended and lamellation fracture in shales from JY-A Well (The depth is 2361 m). This fracture bypassed the mineral particles. (c) One bifurcated and aggregated lamellation fracture in shales from JY-A Well (The depth is 2307.8 m). (d) Lamellation fractures filled with quartz from JY-B Well (The depth is 4039.7 m. Cross-polarized, light color). (For interpretation of the references to color in this figure legend, the reader is referred to the Web version of this article.)

secondary lamellation fractures can be further divided. The secondary lamellation fractures can also converge into one trunk when extending forward. Whether bifurating or converging, lamellation fractures are almost parallel to the surface of lamellation. The fracture aperture of different lamellation fractures varies greatly (Fig. 6d), ranging from 1 μm to 10 mm or even larger. When filled, lamellation fractures can withstand overburden pressure with the support of minerals. The fracture aperture is very large then.

Thin section observations also show that there are magnitude differences in fracture aperture at different locations in one lamellation fracture (Fig. 7d). The fracture aperture at the narrowest point is 8.74 μm (Fig. 7b), while at the widest point it reaches 100.55 μm (Fig. 7f). Under the magnifier with smaller magnification, the fractures are usually discontinuous (Fig. 7d). When the magnification increases,

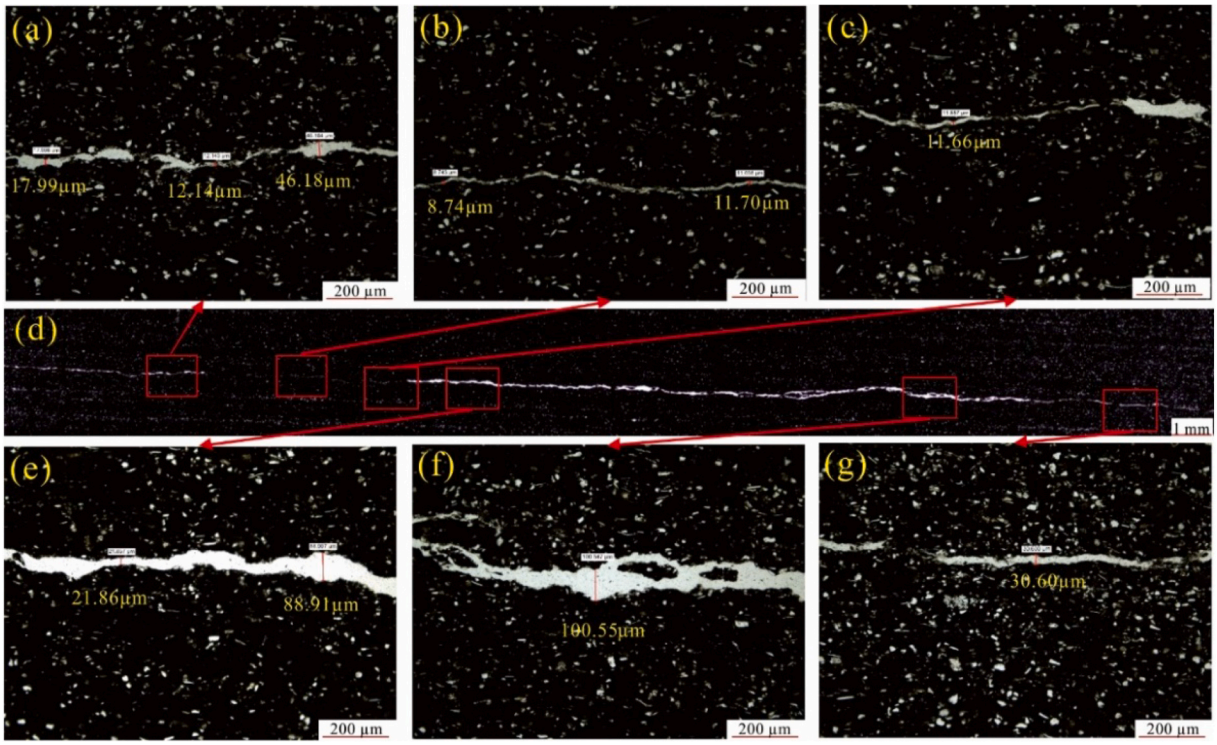

Fig. 7. One lamellation fracture at different magnification levels observed from thin sections of the shales in the Fuling Area. (d) A continuous lamellation fracture in shales from JY-A Well (The depth is 2351.2 m). The lamellation fracture has different apertures in different positions. (a), (b), (c), (e), (f), and (g) are details magnified from parts of (d).

lamellation fractures become continuous (Fig. 7b). Due to the great magnitude differences, more accurate observation methods are needed to characterize lamellation fractures.

SEM observation results show that there are fillings in some lamellation fractures (Fig. 8a and Fig. 8c). Through Energy Dispersive X-Ray Fluorescence Spectrometer (EDX) analysis results (Fig. 8d), these fillings prove to be bitumen mainly (Fig. 8f). A lot of organic matter pores are found in the bitumen (Fig. 8e). These pores have various diameters, ranging from 171.7 nm to 3.7 μm (Fig. 8b), larger than the diameters of general organic matter pores in the shale matrix (Gou et al., 2019; Xu et al., 2020). The conversion from liquid hydrocarbons to gas can lead to a significant increase in volume (Barker, 1990; Wang et al., 2020). Lamellation fractures also provide remarkable space. When the rate of volume increase exceeds the rate of volume loss due to fluid excretion and migration, it may cause overpressure (Li et al., 2016; Gao et al., 2019). Furthermore, overpressure contributes to the preservation of the lamellation fractures and organic matter pores. Therefore, the diameter of the organic matter pores in the lamellation fractures is larger than that of the organic matter pores in the matrix.

4.3. Vertical distribution characteristics of lamellation fractures

Having described the development characteristics of the development of lamellation fractures, this research studied the vertical distribution characteristic of lamellation fractures from a well in the Fuling Area. Taking JY-A Well as an example (Fig. 9), the density of the lamellation fractures is relatively high, ranging from 0.3 cm^{-1} to 1.5 cm^{-1}. The average is about 0.9 cm^{-1}. Generally, the density is decreasing upwards. At the bottom of this well, there are many lamellation fractures in layer ①, where the density is around 1.25 cm^{-1}. The density of lamellation fractures in layers ② to ④ is smaller, with an average of 1.15 cm^{-1}. From layer ⑤ to ⑦, the density decreases significantly, with an average of 1.01 cm^{-1}, 0.75 cm^{-1}, 0.74 cm^{-1}, respectively. Different from this part, the density in layer ⑧ increases, with an average of 0.94 cm^{-1}. For layer ⑨, the density is only 0.63 cm^{-1}, reaching to the minimum. In general, JY-A Well is characterized by obvious trichotomy. Lamellation fractures in the five layers at the bottom are the densest, with density mostly above 1 cm^{-1}. In the middle, the density decreases in layers ⑥ and ⑦, mostly above 0.75 cm^{-1}. At the top, the density increases firstly and then decreases in layers ⑧ and ⑨. In layer ⑨, the density of lamellation fractures is the lowest.

5. Discussions

5.1. Effect of brittle minerals on lamellation fractures

The influence of mineral composition and lithology on fracture development is mainly through their effects on the mechanical properties of shale. Many studies have shown that the shale has a higher content of brittle minerals, such as quartz, carbonate minerals, feldspar, and so on, with high hardness and strong resistance to stress deformation, which corresponds to a higher Young's modulus and a lower Poisson's ratio. For this reason, rocks exhibit greater brittleness when subjected to external forces. Therefore, natural fractures and artificially induced fractures tend to be formed more easily under external stresses (Gale et al., 2014; Zeng et al., 2016; Huo et al., 2018; Zhang et al., 2019; Lawal et al., 2021). Some studies believe that the layered arrangement of brittle minerals in shale leads to laminae and lamellation. These interfaces are weak surfaces in shale. Under stress, it is easy to cause tensile stress concentration, leading to the opening along the bedding plane and expanding in the direction that is most likely to fracture. Finally, each bedding plane expands and connects to form a complex

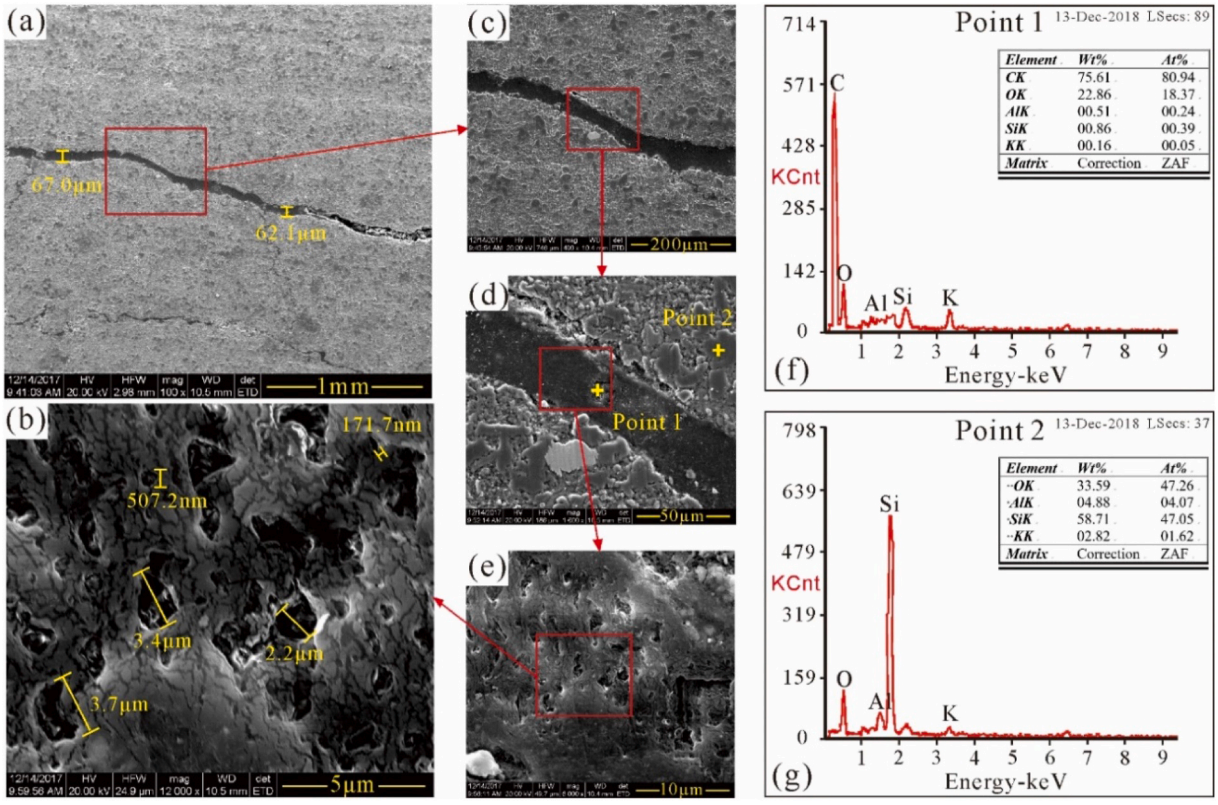

Fig. 8. Microscopic characteristics of lamellation fractures observed through SEM and results of EDX analysis. (a) and (c) show lamellation fractures at different magnification levels observed in SEM from JY-A Well (The depth is 2351.2 m). (b) and (e) show organic matter pores in bitumen. The organic matter pore size ranges from 171.7 nm to 3.7 μm. (d) shows the points from EDX analysis. (f) shows the result of EDX analysis, where point 1 reveals bitumen. (g) shows the result of EDX analysis, where the point 1 indicates quartz.

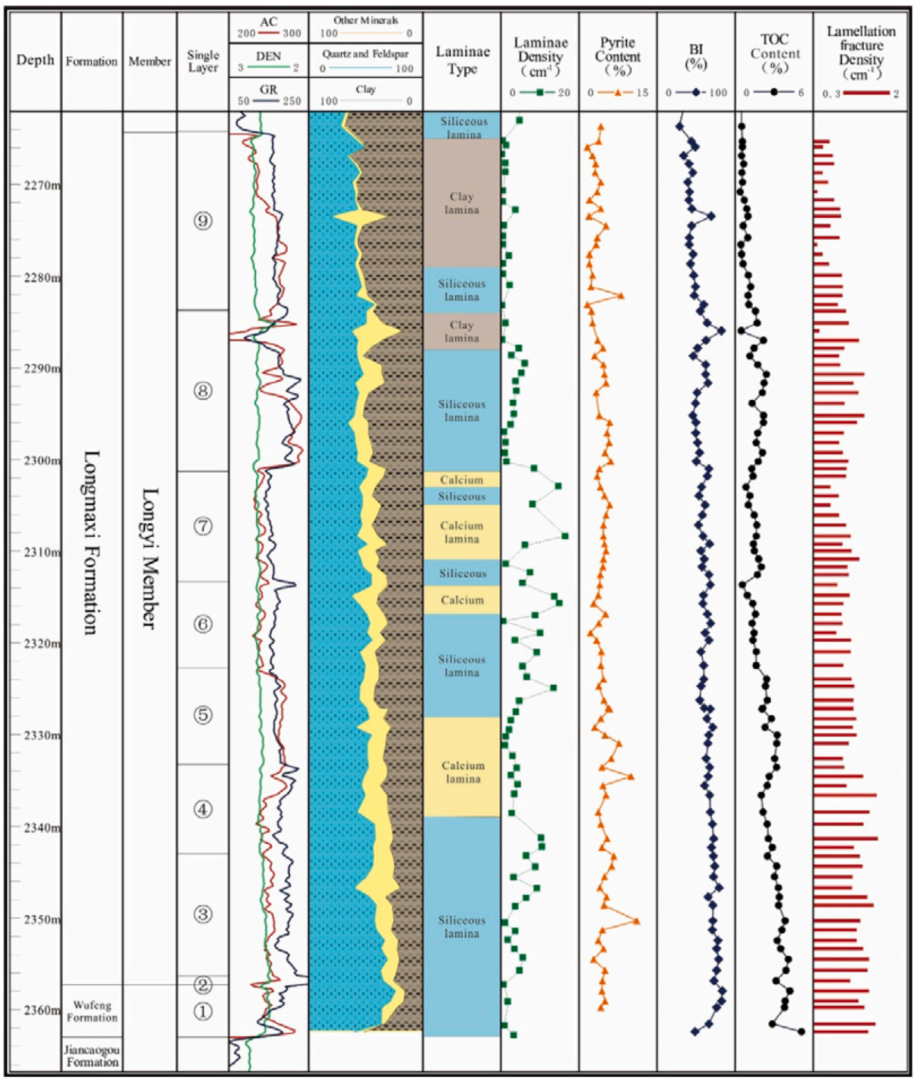

Fig. 9. Comprehensive evaluation in the shales of the Wufeng Fm - the First Member of the Longmaxi Fm from JY-A Well. The fields include the depth, layer division, mineral composition, laminae type, laminae density, BI, TOC content, and lamellation fractures' density (The laminae type and laminae density columns referred to Wang et al., 2019).

fracture, causing macroscopic rupture of rock (Li and Li, 2018; Liu et al., 2020a; Sun et al., 2021). Of course, this is just a simple discussion of the relationship between the content of brittle minerals and slab fractures. The increase in the content of brittle minerals provides more possibilities for the formation of shale fractures. Whether the shale can be broken or not mainly depends on the size of the external force. In the next section, we will give a detailed explanation of geomechanics.

As mentioned in the previous article, we use BI to characterize the content of brittle minerals. According to the statistics in the experiments, the higher the BI is, the more lamellation fractures develop. When BI increases by 10%, the lamellation fracture density increases by 19% (Fig. 10a). When the BI is above 50%, the development degree of

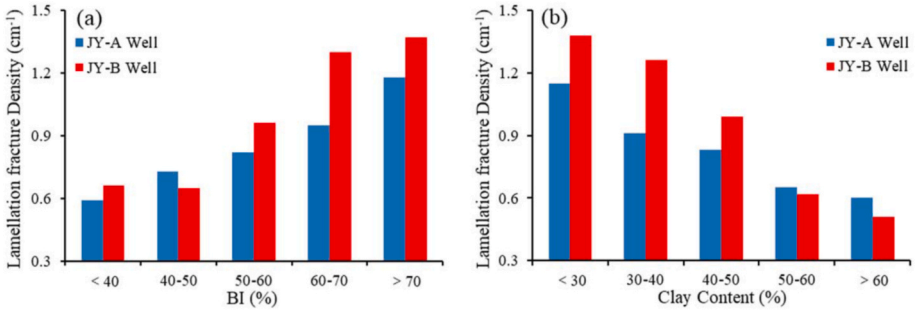

Fig. 10. (a) The relationship between BI and lamellation fracture density in the shales of the Wufeng Fm - the First Member of the Longmaxi Formation from JY-A Well and JY-B Well. (b) The relationship between clay content and lamellation fracture density in the shales of the Wufeng Fm - the First Member of the Longmaxi from JY-A Well and JY-B Well.

lamellation fractures increases significantly. On the other hand, the higher the clay content is, the stronger the plasticity. This makes it harder to form lamellation fractures when rocks are exposed to external forces. According to the data from JY-A Well and JY-B Well, it is found that the higher the clay content is, the lower the density of lamellation fractures is (Fig. 10b).

At the same time, the type of brittle minerals also affects rock properties. In the Fuling Area, the quartz in layers ⑥ and ⑦ originated from the terrestrial debris (Zhao et al., 2017), having no correlation with TOC content (Fig. 11a). The quartz of other layers is mainly derived from the dissolution and reprecipitation materials of biosilica (Zhao et al., 2017), correlating significantly with the TOC content (Fig. 11b). The diagenetic evolution process of authigenic quartz is more complicated than that of terrestrial quartz (Ran et al., 2015), the accumulation of authigenic microcrystalline quartz in the primary pores can suppress the compaction, maintaining the shales to be rigid (Dowey and Taylor, 2017; Zhao et al., 2017). Migrated organic matters filled the associated pore network in authigenic microcrystalline quartz aggregates would more likely generate a better pore pressure through secondary cracking (Zhao et al., 2017). The overpressure caused by the increase of pore pressure is an important condition for the generation of lamellation fractures (Cobbold and Rodrigues, 2007). This study reveals that the BI of layers with terrestrial quartz has no correlation with the density of the lamellation fractures (Fig. 11c), while for layers with authigenic quartz it has a good correlation with the density of the lamellation fractures (Fig. 11d).

5.2. Effect of TOC on lamellation fractures

TOC is an important factor controlling the development of lamellation fractures. Assuming the geomechanical backgrounds, rock mechanical properties, and mineral compositions are the same in the environment, the higher the TOC content is, the easier the lamellation fractures to form (Rozhko et al., 2007; Zeng et al., 2013; Wang et al., 2016). We try to explain how organic matter causes lamellation fractures in shale from the perspective of geomechanics. The fractures produced by tectonic stress are called structural fractures, and they are different from the lamellation fractures in all aspects of morphological characteristics (Zeng et al., 2016). Then it is obvious that the maximum principal stress during the formation of the sheet fracture is not the tectonic stress but the gravity. Organic matters could increase the pore-fluid pressure in the shales during the hydrocarbon generation period, especially in the period when large amounts of gas generated. When the pore-fluid pressure is greater than the hydrostatic pressure of an equivalent free column of water, we called it overpressure (Lash and Engelder, 2005; Jiu et al., 2013; Zhang et al., 2020). The overpressure takes up part of the load, reducing the effective stress on the shales, so that:

$$\sigma'_1 = \sigma_1 - P \quad (2)$$

$$\sigma'_3 = \sigma_3 - P \quad (3)$$

Here P is the overpressure, $\sigma 1$, and σ_3 are the greatest and least values of effective stress, $\sigma' 1$ and $\sigma' 3$ are the greatest and least values of effective stress after the change.

The reduction in effective stress causes the Mohr circle to shift to the left by the amount of overpressure (Fig. 12a), while the size does not change (Jaeger and Cook, 1979). If we consider the flow of fluid, then this situation is too simple. Darcy's law for fluid flow implies that seepage forces modify the general balance of forces on the element. For upward flow, the seepage forces act vertically, not horizontally (Cobbold and Rodrigues, 2007; Cobbold et al., 2013). Hence vertical effective stress also will be reduced by the amount of overpressure. However, the same is not true for the horizontal direction, in which there are no seepage forces (Hillis, 2003; Mourgues and Cobbold, 2003). At this time, the rock still satisfies the elastic deformation, and the relationship between vertical effective stress and horizontal effective stress still conforms to formula (2):

$$\sigma'_3 = \left(\frac{\nu}{1-\nu}\right)\sigma'_1 = \left(\frac{\nu}{1-\nu}\right)(\sigma_1 - P) \quad (4)$$

Here, ν is Poisson's ratio.

As the overpressure increases, the Mohr circle moves to the left and the size becomes smaller. When the overpressure completely cancels out the gravity, all effective stresses would be offset and the Mohr's circle goes back to the origin (Fig. 12b). As the overpressure becomes greater,

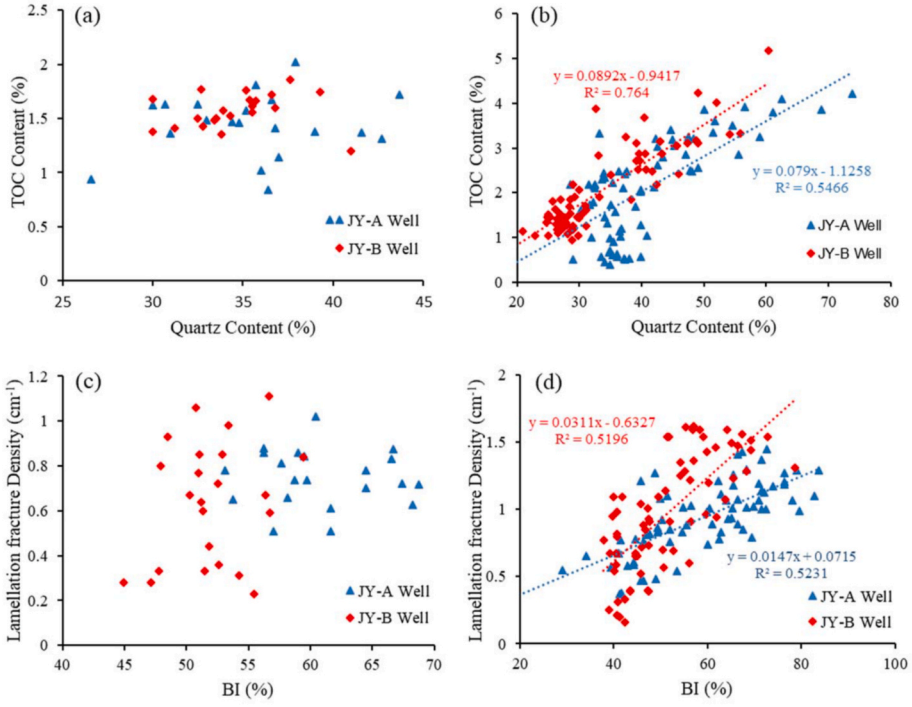

Fig. 11. (a) The relationship between quartz and TOC content in the shales of the layers ⑥ and ⑦ from JY-A Well and JY-B Well. (b) The relationship between quartz and TOC content in the shales of the other layers in the Wufeng Fm - the First Member of the Longmaxi Fm from JY-A Well and JY-B Well. (c) The relationship between BI and lamellation fracture density in the shales of the layers with terrestrial quartz in the Wufeng Fm - the First Member of the Longmaxi Fm from JY-A Well and JY-B Well. (d) The relationship between BI and lamellation fracture density in the shales of the layers with authigenic quartz in the Wufeng Fm - the First Member of the Longmaxi Fm from JY-A Well and JY-B Well.

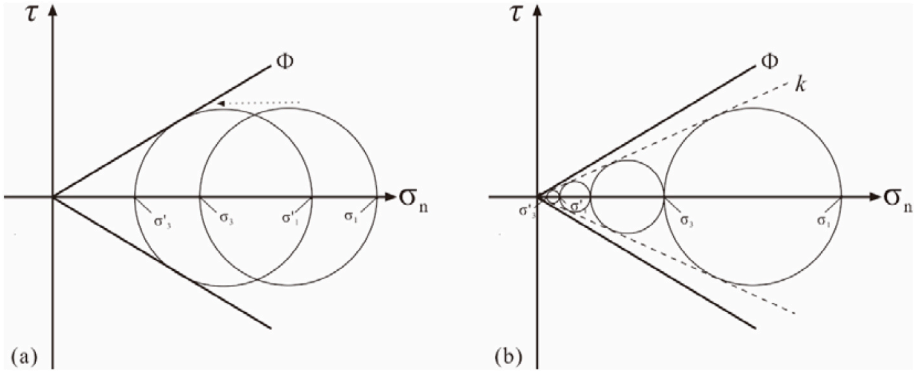

Fig. 12. (a) Influence of increasing overpressure on position of Mohr circle for effective stress. (b) Influence of increasing overpressure on position of Mohr circle for effective stress.

the Mohr's circle will continue to grow in the tensile stress field (Cobbold et al., 2013). When it touches the envelope, lamellation fractures can be formed because of the horizontal tensile failure (Fig. 13). Heng et al. (2020) conducted some rock mechanics experiments on the Wufeng-Longmaxi shale from the outcrop near the Fuling area. Their results showed that the tensile strength, cohesion, internal friction angle of the bedding planes are 4.713 MPa, 8.93 MPa, 31.216°, respectively, which are significantly lower than the rock matrix. Based on these data, we can draw the envelope of the Wufeng-Longmaxi shale.

In addition, the organic matter will yield acid fluids during the maturation process. It can dissolve some minerals to change the sensitivity of the shales (Zeng et al., 2013), which is more conducive to form lamellation fractures. The intrusion of acid fluids dissolves and reforms the original lamellation fractures, extending the fractures (Zhang et al., 2019). Some scholars (Jiu et al., 2013) believe that residual carbon after the evolution of organic matter can improve the brittleness of shales and make the shales more prone to crack.

The statistics show that when the TOC content is less than 2%, the density of lamellation fractures is low. However, when the TOC content is greater than 2%, plenty of lamellation fractures emerge, and the density of lamellation fractures is over 1 cm^{-1} (Fig. 14a). By fitting statistical data, there is a good positive correlation between the TOC content and the density of the lamellation fractures (Fig. 14b). The correlation coefficient in JY-A Well is 0.66, and in JY-B Well is 0.54. Higher TOC percentage reflects widely distributed lamellation fractures. When TOC content increases by 1%, the density of lamellation fractures will increase by an average of 0.26 cm^{-1}. The TOC content is a key factor in controlling the development of lamellation fractures.

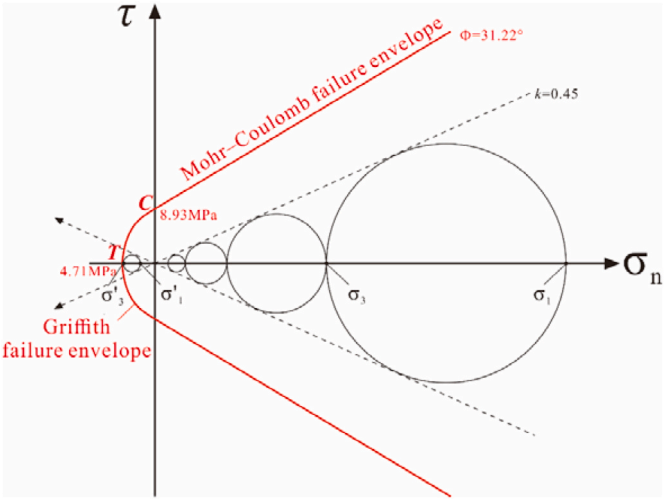

Fig. 13. Mechanical explanation of lamellation fractures' formation under overpressure. In the figure, τ is shear stress; σn is normal stress (Positive values indicate compression and negative values indicate tension); σ1 is Maximum principal stress; σ3 is Minimum principal stress; C is cohesion; T is tensile strength; k is elastic constant, it can be obtained from Young's modulus. (modified from Cobbold et al., 2013).

5.3. *Effect of pyrite on lamellation fractures*

Pyrite is another important factor that affects the formation of lamellation fractures. Compared with other minerals, pyrite acts as an important environmental indicator. It is usually formed in a quiet water body that is anoxic (Raiswell and Canfield, 2012; Mahoney et al., 2019). In the Fuling Area, pyrite content has a good correlation with TOC content (Zhao et al., 2018). During the evolution of organic matters, pyrite also plays a catalytic role (Bakr et al., 1991), thereby accelerates the generation of gas and form more lamellation fractures. Automorphic pyrite in the lamellation fractures provides support to the fractures and keep the fracture aperture open. Statistics on JY-A Well and JY-B Well show that a higher pyrite content results in more lamellation fractures (Fig. 15). When the pyrite content is greater than 3%, numerous lamellation fractures emerge. An increase in the pyrite content of 1% can increase the lamellation fracture density by 9%.

5.4. *Effect of laminae on lamellation fractures*

There are plenty of laminae in marine shales in the Fuling Area. Wang et al. (2019) divided the laminae type in the Wufeng Fm - Longmaxi Fm in JY-A Well into siliceous laminae, calcareous laminae, and clay laminae, then counted laminae density. Based on their results, the authors studied the relationship between the laminae and lamellation fractures. The statistical results show that there are more lamellation fractures in siliceous laminae and calcareous laminae (Fig. 16a), with an average laminae density of 1.01 cm^{-1} and 0.96 cm^{-1}, respectively. Meanwhile, there are few lamellation fractures in clay laminae. The average laminae density is only 0.66 cm^{-1}. The laminae type determines the development of lamellation fractures. As siliceous laminae and calcareous laminae show stronger brittleness, they are more suitable for lamellation fractures to form.

The statistics of JY-A Well (Fig. 16b) show that an appropriate laminae density results in a high density of lamellation fractures. For example, the fracture density is the largest when laminae density is about 3-4cm-1 in the study area. By fitting the statistical data, laminae density does not have a clear relation with lamellation fractures in general (Fig. 16c). But when focusing on the range between 0 and 4 cm^{-1}, it is shown that obvious positive correlation between laminae density and lamellation fractures with a correlation coefficient of 0.48. There are more lamellation fractures in the shales with higher laminae density (Fig. 16d). When the density of the laminae is greater than 4

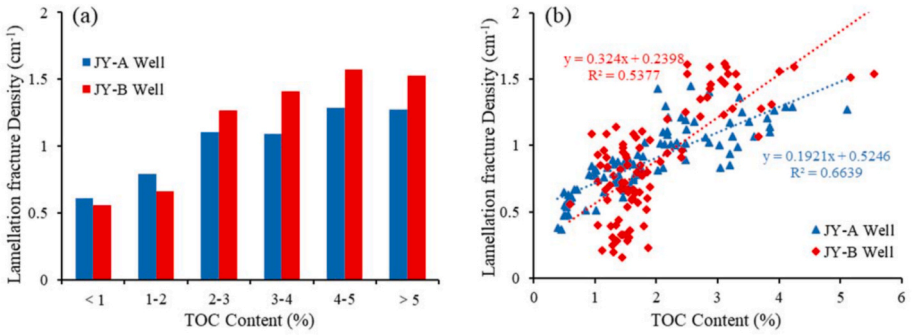

Fig. 14. The relationship between TOC content and lamellation fracture density in the shales of the Wufeng Fm - the First Member of the Longmaxi Fm in JY-A Well and JY-B Well. (a) shows the relationship between TOC content and lamellation fracture density under segmented statistics. (b) The relationship between TOC content and lamellation fracture density under scatter intersection statistics.

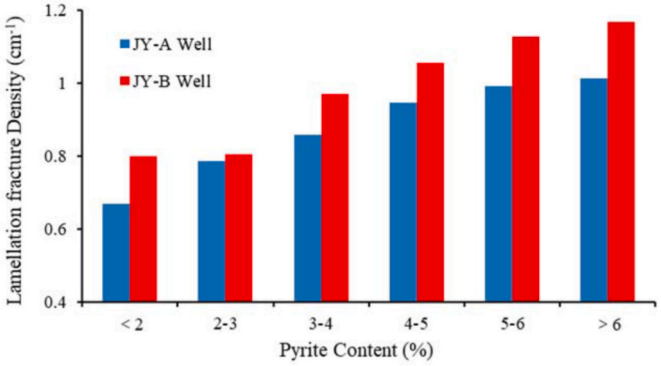

Fig. 15. The relationship between pyrite content and lamellation fracture density in the shales of the Wufeng Fm - the First Member of the Longmaxi Fm from JY-A Well and JY-B Well.

cm^{-1}, the degree of development of the lamellation fractures will not increase accordingly, the density of lamellation fractures remains around 1 cm-1. In general, the lamina interface is a mechanically weak surface. It is easy to break and form fractures when subjected to external forces (Jiu et al., 2013; Zhang et al., 2020). However, densely distributed laminae usually reflect a more turbulent and oxygen-rich paleo--environment or influx of seasonal terrestrial debris (Shi et al., 2018; Wang et al., 2019). Such a sedimentary environment is adverse to the accumulation of organic matter to its swift currents (Yawar and Schieber, 2017). Even if the organic-poor shale formed in this sedimentary environment has high laminae density, but they lack the overpressure caused by the evolution of organic matter, it is not conducive to the formation of lamellation fractures Shi et al., 2020b). Therefore, higher laminae density contributes to denser lamellation fractures when the laminae density is in a certain range. Too densely-distributed laminae will suppress the formation of lamellation fractures.

6. Conclusions

(1) Lamellation fractures are widely distributed in the marine shales of the Wufeng Formation and the First Member of the Longmaxi Formation in the Fuling Area, Eastern Sichuan Basin. Lamellation fractures are parallel to the lamellations, which can be partially curved, bifurcated, converged, and dissolved. The fracture apertures generally range from 1 μm to 500 μm, with a peak value of

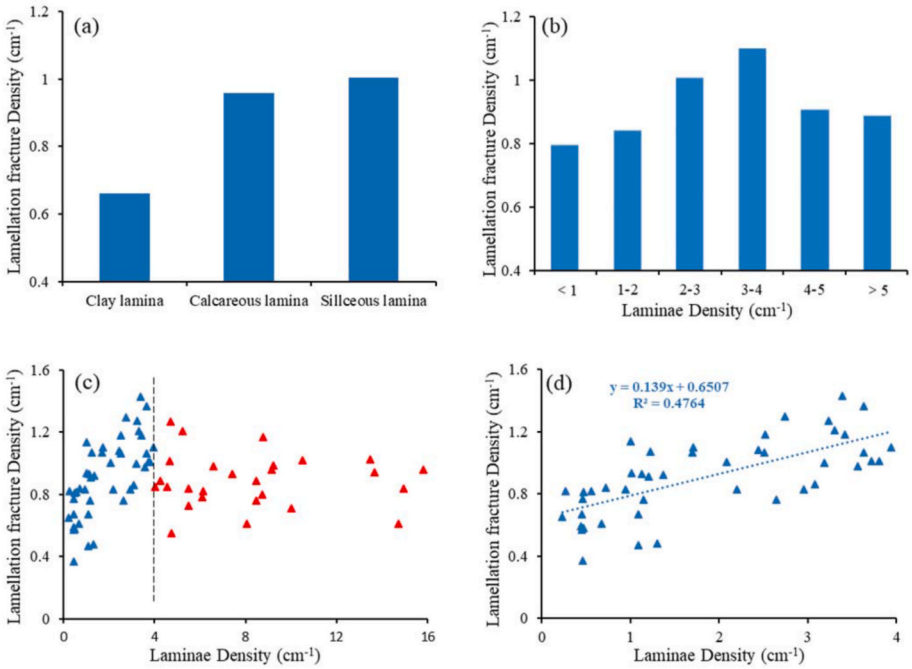

Fig. 16. The relationship between laminae and lamellation fractures in the shales of the Wufeng Fm - the First Member of the Longmaxi Fm **from JY-A Well. (a) shows the relationship between laminae type and lamellation fracture density.** (b) shows the relationship between laminae density and lamellation fracture density under segmented statistics. (c) reflects the relationship between laminae density and lamellation fracture density under scatter intersection statistics. **(d) shows the relationship between laminae density and lamellation fractures density when laminae density is less than 4 cm^{-1}. (The laminae type and laminae density columns are referred to Wang et al., 2019).**

around 100 μm. Even though the lamellation fractures are almost continuous, there are magnitude differences in fracture aperture at different locations in one lamellation fracture. Less than 1% of the lamellation fractures are filled with quartz, calcite, pyrite, and bitumen. The width of the filling veins is generally between 100 and 1000 μm, with the maximum reaching 1 cm. The organic pores in the filled bitumen is larger than those in the matrix.

(2) The development degree of lamellation fractures is controlled by brittle minerals, TOC, laminae, and pyrite. Brittle minerals, especially authigenic quartz, is an important controlling factor to the development of lamellation fractures. When BI increases by 10%, the lamellation fracture density will increase by 19%. The organic matters control the formation and evolution of lamellation fractures by generating gas and resulting in overpressure. Simultaneously, the acid fluids produced by hydrocarbon generation will also reform the lamellation fractures. An increase in the TOC content of 1% can increase the lamellation fracture density by 0.26 cm^{-1}. In addition, higher pyrite content facilitates the development of lamellation fractures. Lamellation fracture density will increase by 9% with pyrite content increased by 1%. At last, siliceous and calcareous laminae in shales are more suitable for lamellation fractures to develop. When the laminae density is smaller than 4 cm^{-1}, it is easier to develop lamellation fractures with higher laminae density. However, too densely-distributed laminae will suppress the formation of lamellation fractures. Among all factors above, TOC is the main one that affects the development of lamellation fractures.

(3) The density of lamellation fractures is between 0.2 cm^{-1} and 2 cm^{-1}. Obvious differences appear vertically. The density of lamellation fractures decreases from the bottom to the top. The lamellation fractures in five layers at the bottom are densest, with density mostly above 1 cm^{-1} due to the high TOC and pyrite content, great brittleness, and moderate laminae density.

Credit author statement

Xiang Xu: Conceptualization, Formal analysis, Writing – original draft. **Lianbo Zeng**: Supervision, Conceptualization, Writing – review & editing. **He tian**: Data curation, Resources, Investigation. **Kegang Ling**: Writing – review & editing. **Shiqi Che**: Resources, Visualization. **Xiao Yu**: Writing – review & editing. **Zhiguo Su**: Data curation, Project administration. **Shaoqun Dong**: Writing – review & editing.

Declaration of competing interest

The authors declare that they have no known competing financial interests or personal relationships that could have appeared to influence the work reported in this paper.

Acknowledgments

The authors would like to thank the Research Institute of Petroleum Exploration and Development of SINOPEC Jianghan Oilfield Company, for constructive help. The financial supports by the National Natural Science Foundation of China (Grant No. U1663203), China Scholarship Council and Science Foundation of China University of Petroleum, Beijing (Grant No. 2462020XKJS02) are greatly appreciated.

Appendix A. Supplementary data

Supplementary data to this article can be found online at https://doi.org/10.1016/j.petrol.2021.109091.

References

Allan, A.M., Vanorio, T., Dahl, J.E., 2014. Pyrolysis-induced P-wave velocity anisotropy in organic-rich shales. Geophysics 79, 41–53.
Anders, M.H., Laubach, S.E., Scholz, C.H., 2014. Microfractures: a review. J. Struct. Geol. 69 (12), 377–394.
Barker, C., 1990. Calculated volume and pressure changes during the thermal cracking of oil to gas in reservoirs. AAPG (Am. Assoc. Pet. Geol.) Bull. 74, 1254–1261.
Bakr, M.Y., Yokono, T., Sanada, Y., Akiyama, M., 1991. Role of pyrite during the thermal degradation of kerogen using in Situ high-temperature ESR technique. Energy Fuels 5, 441–444.
Bons, P.D., Elburg, M.A., Gomez-Rivas, E., 2012. A review of the formation of tectonic veins and their microstructures. J. Struct. Geol. 43, 33–62.
Cobbold, P.R., Rodrigues, N., 2007. Seepage forces, important factors in the formation of horizontal hydraulic fractures and bedding-parallel fibrous veins ("beef" and "cone-in-cone"). Geofluids 7, 313–332.
Cobbold, P.R., Zanella, A., Rodrigues, N., Loseth, H., 2013. Bedding-parallel fibrous veins (beef and cone-in-cone): worldwide occurrence and possible significance in terms of fluid overpressure, hydrocarbon generation and mineralization. Mar. Petrol. Geol. 43, 1–20.
Dewhurst, D.N., Siggins, A.F., Sarout, J., Raven, M., Nordgard-Bolas, H.M., 2011. Geomechanical and ultrasonic characterization of a Norwegian Sea shale. Geophysics 76, 101–111.
Dowey, P.J., Taylor, K.G., 2017. Extensive authigenic quartz overgrowths in the gas-bearing Haynesville-Bossier Shale. USA. Sediment. Geol. 356, 15–25.
Fatahi, H., Hossain, M.M., Sarmadivaleh, M., 2017. Numerical and experimental investigation of the interaction of natural and propagated hydraulic fracture. J. Nat. Gas Sci. Eng. 37, 409–424.
Ferrill, D.A., Morris, A.P., Hennings, P.H., Haddad, D.E., 2014. Faulting and fracturing in shale and self-sourced reservoirs: Introduction. AAPG (Am. Assoc. Pet. Geol.) Bull. 98 (11), 2161–2164.
Gale, J.F.W., Reed, R.M., Holder, J., 2007. Natural fractures in the Barnett Shale and their importance for hydraulic fracture treatments. AAPG Bull. 91 (4), 603–622.
Gale, J.F.W., Holder, J., 2010. Natural fractures in some US shales and their importance for gas production. Geol. Soc. Londn. Petrol. Geol. Conf. Ser. 7, 1131–1140.
Gale, J.F.W., Laubach, S.E., Olson, J.E., Eichhubl, P., Fall, A., 2014. Natural fractures in shale: a review and new observations. AAPG Bull. 98, 2165–2216.
Gao, J., Zhang, J.K., He, S., Zhao, J.X., Li, W., 2019. Overpressure generation and evolution in Lower Paleozoic gas shales of the Jiaoshiba region, China: implications for shale gas accumulation. Mar. Petrol. Geol. 102, 844–859.
Gholami, R., Rasouli, V., Sarmadivaleh, M., Minaeian, V., Fakhari, N., 2016. Brittleness of gas shale reservoirs: a case study from the north Perth basin, Australia. J. Nat. Gas Sci. Eng. 33, 1244–1259.
Gong, L., Su, X.C., Gao, S., Fu, X.F., Jabbari, H., Wang, X.X., Liu, B., Yue, W.T., Wang, Z. S., Gao, A., 2019. Characteristics and formation mechanism of natural fractures in the tight gas sandstones of Jiulongshan gas field, China. J. Petrol. Sci. Eng. 175, 1112–1121.
Gou, Q.Y., Xu, S., Hao, F., Yang, F., Zhang, B.Q., Shu, Z.G., Zhang, A.H., Wang, Y.X., Lu, Y.B., Cheng, X., Qing, J.W., Gao, M.T., 2019. Full-scale pores and micro-fractures characterization using FE-SEM, gas adsorption, nano-CT and micro-CT: a case study of the Silurian Longmaxi Formation shale in the Fuling area, Sichuan Basin, China. Fuel 253, 167–179.
Gou, Q.Y., Xu, S., Hao, F., Zhang, B.Q., Li, Q.Q., 2020. Quantitative calculated shale gas contents with different lithofacies: a case study of Fuling gas shale, Sichuan Basin, China. J. Nat. Gas Sci. Eng. 76, 103222.
Gratier, J.-P., Frery, E., Deschamps, P., Røyne, A., Renard, F., Dysthe, D., Ellouz-Zimmerman, N., Hamelin, B., 2012. How travertine veins grow from top to bottom and lift the rocks above them: the effect of crystallization force. Geology 40, 1015–1018.
Gu, Y., Ding, W.L., Tian, Q.N., Xu, S., Jiao, B.C., 2020. Developmental characteristics and dominant factors of natural fractures in lower Silurian marine organic-rich shale reservoirs: a case study of the Longmaxi formation in the Fenggang block, southern China. J. Petrol. Sci. Eng. 192, 107277.
Guo, T.L., Zhang, H.R., 2014. Formation and enrichment mode of Jiaoshiba shale gas field, Sichuan Basin. Petrol. Explor. Dev. 41 (1), 31–40.
Guo, X.S., 2019. Major factors controlling the shale gas accumulations in Wufeng-Longmaxi Formation of the Pingqiao shale gas field in fuling area, Sichuan Basin, China. J. Nat. Gas Geosci. 4 (3), 129–138.
Heng, S., Li, X., Liu, X., Chen, Y., 2020. Experimental study on the mechanical properties of bedding planes in shale. J. Nat. Gas Sci. Eng. 76, 103161.
Hill, D.G., Nelson, C.R., 2000. Gas productive fractured shales: an overview and update. Gas Tips Gas Res. Inst. 6 (2), 4–13.
Hillis, R.R., 2003. Pore Pressure/stress Coupling and its Implications for Rock Failure, vol. 216. Geological Society of London Special Publication, pp. 359–368.
Holt, R.M., Fjær, E., Stenebråten, J.F., Nes, O.M., 2015. Brittleness of shales: relevance to borehole collapse and hydraulic fracturing. J. Petrol. Sci. Eng. 131, 200–209.
Hooker, J.N., Laubach, S.E., Marrett, R., 2013. Fracture-aperture size-frequency, spatial distribution, and growth processes in strata-bounded and non-strata-bounded fractures, Cambrian Meson Group, NW Argentina. J. Struct. Geol. 54, 54–71.
Hu, D.F., Zhang, H.R., Ni, K., Yu, G.C., 2014. Main controlling factors for gas preservation conditions of marine shales in southeastern margins of the Sichuan Basin. Nat. Gas. Ind. B. 1 (2), 178–184.
Hu, M., Huang, W.B., Li, J.Y., 2018. Effects of structural characteristics on the productivity of shale gas wells: a case study on the Jiaoshiba Block in the Fuling shale gasfield, Sichuan Basin. Nat. Gas. Ind. B. 5 (2), 139–147.

Huo, Z., Zhang, J., Li, P., Tang, X., Yang, X., Qiu, Q., Dong, Z., Li, Z., 2018. An improved evaluation method for the brittleness index of shale and its application — a case study from the southern north China basin. J. Nat. Gas Sci. Eng. 59, 47–55.
Jaeger, J.C., Cook, N.G.W., 1979. Fundamentals of Rock Mechanics, third ed. Chapman & Hall, London, p. 593.
Jiang, S., Tang, X.L., Long, S.X., Mclennan, J., Jiang, Z.L., Jiang, Z.Q., Xu, Z.Y., Chen, L., Xue, G., Shi, X., He, Z.L., 2017. Reservoir quality, gas accumulation and completion quality assessment of Silurian Longmaxi marine shale gas play in the Sichuan Basin, China. J. Nat. Gas Sci. Eng. 39, 203–215.
Jiu, K., Ding, W.L., Huang, W.H., Zhang, Y.Q., Zhao, S., Hu, L.J., 2013. Fractures of lacustrine shale reservoirs, the zhanhua depression in the bohai bay basin, eastern China. Mar. Petrol. Geol. 48, 113–123.
John, B.C., 2008. Reservoir characteristics and production potential of woodford Shale. World Oil 8, 83–88.
Kassis, S., Sondergeld, C.H., 2010. Fracture permeability of gas shale: effects of roughness, fracture offset, proppant, and effective stress. Soc. Petrol. Eng. J. 131376, 1–17.
Lander, R.H., Laubach, S.E., 2015. Insights into rates of fracture growth and sealing from a model for quartz cementation in fractured sandstones. GSA (Geol. Soc. of Am.) Bull. 127 (3–4), 516–538.
Lash, G.G., Engelder, T., 2005. An analysis of horizontal microcracking during catagenesis: example from the Catskill delta complex. AAPG (Am. Assoc. Pet. Geol.) Bull. 89 (11), 1433–1449.
Laubach, S.E., Olson, J.E., Cross, M.R., 2009. Mechanical and fracture stratigraphy. AAPG (Am. Assoc. Pet. Geol.) Bull. 93 (11), 1413–1426.
Lawal, L.O., Mahmoud, M., Adebayo, A., Sultan, A., 2021. Brittleness and microcracks: a new approach of brittleness characterization for shale fracking. J. Nat. Gas Sci. Eng. 87.
Li, J., Li, W., 2018. A quantitative seismic prediction technique for the brittleness index of shale in the Jiaoshiba Block, Fuling shale gas field in the Sichuan Basin. Nat. Gas. Ind. B 5, 1–7.
Li, S.J., Yuan, Y.S., Sun, W., Sun, D.S., Jin, Z.J., 2016. Formation and destruction mechanism as well as major controlling factors of the Silurian shale gas overpressure in the Sichuan Basin, China. J. Nat. Gas Geosci. 1 (4), 287–294.
Liu, B., Wang, S., Ke, X., Fu, X., Liu, X., Bai, Y., Pan, Z., 2020a. Mechanical characteristics and factors controlling brittleness of organic-rich continental shales. J. Petrol. Sci. Eng. 194.
Liu, G.P., Zeng, L.B., Li, H.N., Ostadhassan, M., Rabiei, M., 2020b. Natural fractures in metamorphic basement reservoirs in the Liaohe Basin, China. Mar. Petrol. Geol. 119, 104479.
Luo, Y., Liu, H.P., Zhao, Y.C., Wang, G.C., 2016. Effects of gas generation on stress states during burial and implications for natural fracture development. J. Nat. Gas Sci. Eng. 30, 295–304.
Lyu, W.Y., Zeng, L.B., Zhang, B.J., Miao, F.B., Lyu, P., Dong, S.Q., 2017. Influence of natural fractures on gas accumulation in the Upper Triassic tight gas sandstones in the northwestern Sichuan Basin, China. Mar. Petrol. Geol. 83, 60–72.
Mahoney, C., März, C., Buckman, J., Wagner, T., Blanco-Velandia, V.O., 2019. Pyrite oxidation in shales: implications for palaeo-redox proxies based on geochemical and SEM-EDX evidence. Sediment. Geol. 3891, 186–199.
Marrett, R., Ortega, O.J., Kelsey, C.M., 1999. Extent of power-law scaling for natural fractures in rock. Geology 27 (9), 799–802.
Mourgues, R., Cobbold, P.R., 2003. Some tectonic consequences of fluid overpressures and seepage forces as demonstrated by sandbox modelling. Tectonophysics 376, 75–97.
Nie, H.K., Li, D.H., Liu, G.X., Lu, Z.Y., Wang, H., Wang, R.Y., Zhang, G.R., 2020. An overview of the geology and production of the Fuling shale gas field, Sichuan Basin, China. Energy Geosci. 1 (3–4), 147–164.
Ortega, O.J., Marrett, R.A., Laubach, S.E., 2006. A scale-independent approach to fracture intensity and average spacing measurement. AAPG (Am. Assoc. Pet. Geol.) Bull. 90 (2), 193–208.
Raiswell, R., Canfield, D.E., 2012. The iron biogeochemical cycle past and present. Geochem. Pers. 1 (1), 1–2.
Rasouli, V., Sutherland, A., 2014. Geomechanical characteristics of gas shales: a case study in the north perth basin. J. Rock Mech. Rock Eng. 47 (6), 2031–2046.
Ran, B., Liu, S.G., Jansa, L., Sun, W., Yang, D., Ye, Y.H., Wang, S.Y., Luo, C., Zhang, X., Zhang, C.J., 2015. Origin of the upper ordovicianelower silurian cherts of the Yangtze block, south China, and their palaeogeographic significance. J. Asian Earth Sci. 108, 1–17.
Rozhko, A.Y., Podladchikov, Y.Y., Renard, F., 2007. Failure patterns caused by localized rise in pore-fluid overpressure and effective strength of rocks. Geophys. Res. Lett. 34, 22304.
Shi, Z.S., Qiu, Z., Dong, D.Z., Lu, B., Zhang, M.Q., 2018. Lamina characteristics of gas-bearing shale fine-grained sediment of the silurian Longmaxi Formation of well wuxi 2 in Sichuan Basin, SW China. Petrol. Explor. Dev. 45 (2), 358–368.
Shi, J.X., Zeng, L.B., Zhao, X.Y., Zhang, Y.Z., Wang, J.P., 2020a. Characteristics of natural fractures in the upper Paleozoic coal bearing strata in the southern Qinshui Basin, China: implications for coalbed methane (CBM) development. Mar. Petrol. Geol. 113, 104152.
Shi, Z., Dong, D., Wang, H., Sun, S., Wu, J., 2020b. Reservoir characteristics and genetic mechanisms of gas-bearing shales with different laminae and laminae combinations: a case study of Member 1 of the Lower Silurian Longmaxi shale in Sichuan Basin, SW China. Petrol. Explor. Dev. 47, 888–900.
Sone, H., Zoback, M.D., 2014. Viscous relaxation model for predicting least principal stress magnitudes in sedimentary rocks. J. Petrol. Sci. Eng. 124, 416–431.
Sun, W., Zuo, Y., Wu, Z., Liu, H., Zheng, L., Shui, Y., Xi, S., Lou, Y., Luo, X., 2021. The distribution characteristics of brittle minerals in the Lower Cambrian Niutitang Formation in northern Guizhou. J. Nat. Gas Sci. Eng. 86.
Tian, H., Zeng, L.B., Xu, X., Shu, Z.G., Peng, Y.M., Mao, Z., Luo, B., 2020. Characteristics of natural fractures of marine shale and their influence on shale gas in Fuling area, Sichuan Basin. Oil Gas Geol. 42 (3), 474–483 (in Chinese with English abstract).
Tuo, J.C., Wu, C.J., Zhang, M.F., 2016. Organic matter properties and shale gas potential of Paleozoic shales in Sichuan Basin, China. J. Nat. Gas Sci. Eng. 28 (2016), 434–446.
Wang, D.B., Ge, H.K., Wang, X.Q., Wang, J.B., Meng, F.B., Suo, Y., Han, P., 2015. A novel experimental approach for fracability evaluation in tight-gas reservoirs. J. Nat. Gas Sci. Eng. 23, 239–249.
Wang, R.Y., Ding, W.L., Zhang, Y.Q., Wang, Z., Wang, X.H., He, J.H., Zeng, W.T., Dai, P., 2016. Analysis of developmental characteristics and dominant factors of fractures in Lower Cambrian marine shale reservoirs: a case study of Niutitang formation in Cen'gong block, southern China. J. Petrol. Sci. Eng. 138, 31–49.
Wang, X.H., Wang, R.Y., Ding, W.L., Yin, S., Li, Q., 2017. Development characteristics and dominant factors of fractures and their significance for shale reservoirs: a case study from Є1b2 in the Cen'gong block, southern China. J. Petrol. Sci. Eng. 159, 988–999.
Wang, C., Zhang, B.Q., Hu, Q.H., Shu, Z.G., Sun, M.D., Bao, H.Y., 2019. Laminae characteristics and influence on shale gas reservoir quality of lower Silurian Longmaxi Formation in the Jiaoshiba area of the Sichuan Basin, China. Mar. Petrol. Geol. 109, 839–851.
Wang, X.M., Jiang, Z.X., Jiang, S., Chang, J.Q., Li, X.H., Wang, X., Zhu, L., 2020. Pore evolution and formation mechanism of organic-rich shales in the whole process of hydrocarbon generation: study of artificial and natural shale samples. Energy Fuel. 34 (1), 332–347.
Xu, S., Gou, Q.Y., Hao, F., Zhang, B.Q., Shu, Z.G., Lu, Y.B., Wang, Y.X., 2020. Shale pore structure characteristics of the high and low productivity wells, Jiaoshiba shale gas field, Sichuan Basin, China: dominated by lithofacies or preservation condition? Mar. Petrol. Geol. 114, 104211.
Yawar, Z., Schieber, J., 2017. On the origin of silt laminae in laminated shales. Sediment. Geol. 360, 22–34.
Yi, J.Z., Bao, H.Y., Zheng, A.W., Zhang, B.Q., Shu, Z.G., Li, J.Q., Wang, C., 2019. Main factors controlling marine shale gas enrichment and high-yield wells in South China: a case study of the Fuling shale gas field. Mar. Petrol. Geol. 103, 114–125.
Zeng, L.B., Jiang, J.W., Yang, Y.L., 2010. Fractures in the low porosity and ultra-low permeability glutenite reservoirs: a case study of the late Eocene Hetaoyuan formation in the Anpeng Oilfield, Nanxiang Basin, China. Mar. Petrol. Geol. 27, 1642–1650.
Zeng, W.T., Zhang, J.C., Ding, W.L., Zhao, S., Zhang, Y.Q., Liu, Z.J., Jiu, K., 2013. Fracture development in Paleozoic shale of Chongqing area (South China). Part one: fracture characteristics and comparative analysis of main controlling factors. J. Asian Earth Sci. 75, 251–266.
Zeng, L.B., Lyu, W.Y., Li, J., Zhu, L.F., Weng, J.Q., Yue, F., Zu, K.W., 2016. Natural fractures and their influence on shale gas enrichment in Sichuan Basin, China. J. Nat. Gas Sci. Eng. 30, 1–9.
Zhang, B.Q., Meng, Z.Y., Liu, L., Li, K., Shu, Z.H., 2018a. Significance of shale gas genesis to the development of guanyinqiao member, Wufeng Formation, fuling area, Sichuan Basin. Petrol. Geol. Exp. 40 (1), 30–43.
Zhang, L.C., Lu, S.F., Jiang, S., Xiao, D.S., Chen, L., Liu, Y., Zhang, Y.Y., Li, B., Gong, C., 2018b. Effect of shale lithofacies on pore structure of the Wufeng – longmaxi shale in southeast chongqing, China. Energy Fuel. 32, 6603–6618.
Zhang, Y.Y., He, Z.L., Jiang, S., Lu, S.F., Xiao, D.S., Chen, G.H., Li, Y.C., 2019. Fracture types in the lower Cambrian shale and their effect on shale gas accumulation, Upper Yangtze. Mar. Petrol. Geol. 99, 282–291.
Zhang, X.M., Shi, W.Z., Hu, Q.H., Zhai, G.Y., Bai, L.H., 2020. Developmental characteristics and controlling factors of natural fractures in the lower paleozoic marine shales of the upper Yangtze Platform, southern China. J. Nat. Gas Sci. Eng. 30, 103191.
Zhao, W.Z., Li, J.Z., Yang, T., Wang, S.F., Huang, J.L., 2016. Geological difference and its significance of marine shale gases in South China. Petrol. Explor. Dev. 43 (4), 547–559.
Zhao, J.H., Jin, Z.K., Jin, Z.J., Wen, X., Geng, Y.K., 2017. Origin of authigenic quartz in organic-rich shales of the Wufeng and longmaxi formations in the Sichuan Basin, south China: implications for pore evolution. J. Nat. Gas Sci. Eng. 38, 21–38.
Zhao, D.F., Guo, Y.H., Zhu, Y.M., Wang, G., Liu, J., Chong, X., Zhang, J.X., 2018. Micropore characteristics and geological significance of pyrite in shale rocks of Longmaxi Formation. ACTA Sedimental. Sin. 36 (5), 855–876.